Journal Pre-proof

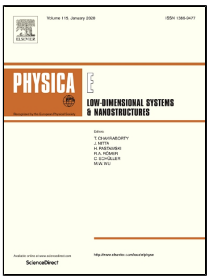

Electrical conductivity and magnetoresistance in twisted graphene electrochemically decorated with Co particles

A.K. Fedotov, S.L. Prischepa, J.A. Fedotova, V.G. Bayev, Arash Ronassi Ali, I.V. Komissarov, N.G. Kovalchuk, S.A. Vorobyova, O.A. Ivashkevich

PII:	S1386-9477(19)31363-3
DOI:	https://doi.org/10.1016/j.physe.2019.113790
Reference:	PHYSE 113790
To appear in:	*Physica E: Low-dimensional Systems and Nanostructures*
Received Date:	09 September 2019
Accepted Date:	18 October 2019

Please cite this article as: A.K. Fedotov, S.L. Prischepa, J.A. Fedotova, V.G. Bayev, Arash Ronassi Ali, I.V. Komissarov, N.G. Kovalchuk, S.A. Vorobyova, O.A. Ivashkevich, Electrical conductivity and magnetoresistance in twisted graphene electrochemically decorated with Co particles, *Physica E: Low-dimensional Systems and Nanostructures* (2019), https://doi.org/10.1016/j.physe.2019.113790

Research paper

Electrical conductivity and magnetoresistance in twisted graphene electrochemically decorated with Co particles

Fedotov A.K. [1,2], Prischepa S.L. [3,6], Fedotova J.A.* [1], Bayev V.G. [1], Ali Arash Ronassi[4], Komissarov I.V. [3,6], Kovalchuk N.G. [3], Vorobyova S.A. [5], Ivashkevich O.A. [5]

[1] Institute for Nuclear Problems of Belarusian State University, Bobruiskaya str. 11, Minsk, 220006, Belarus

[2] Belarusian State University, Nezavisimostci av. 4, 220006, Minsk, Belarus

[3] Belarusian State University of Informatics and Radioelectronics, P. Browka str. 6, 220013 Minsk, Belarus

[4]Payaame Noor University in Borujerd, PO BOX 19395-3697, Tehran, Iran

[5] Research Institute for Physical Chemical Problems of the Belarusian State University, Leningradskaya str. 9, Minsk, 220006, Belarus

[6]National Research Nuclear University (MEPhI), Kashirskoe Highway 31, Moscow 115409, Russia

*Corresponding author. Tel: +375 29 632 60 75. E-mail: Julia@hep.by (Julia Fedotova)

Highlights

- Distributed shunts and high-quality low-ohmic Co electrodes are formed on twisted CVD graphene (*G*) sheets by decoration with Co particles for application in magnetic sensing
- The crossover from negative to positive magnetoresistance in Co-*G*/SiO_2 samples at weak and strong magnetic fields, correspondingly, are considered within the phenomenological model assuming the additional distortion of current-conducting routes under the influence of Lorentz force due to the enhancement of large-scale potential relief enhanced by Co particles.

Abstract

Application of magnetic metal/graphene hybrid structures in magnetosensorics requires the formation of high-quality low-ohmic (barrier-free) contacts and understanding of mechanisms of electric charge transfer near and through the metal/graphene contact area. In present paper we fabricate samples of twisted graphene electrochemically decorated with Co particles (Co-G/SiO_2) which demonstrate perfect ohmic electric contact between Co and graphene sheets. Temperature and magnetic field dependencies of surface resistance for pure twisted graphene (G/SiO_2) and Co-G/SiO_2 samples are considered within the models of 3D Mott variable range hopping and 2D weak-localization quantum corrections to the Drude conductivity. Phenomenological model is proposed explaining the experimentally observed transition from predominantly negative magnetoresistive effect in weak magnetic fields B (below 1-2 T) to positive magnetoresistance (PMR) at B beyond 5 T assuming the growth of PMR due to the distortion of current-conducting routes under the influence of Lorentz force which originates from the enhancement of large-scale potential relief in Co-G/SiO_2 sample. This work considers the new approach to the application of G/SiO_2 decoration with Co particles for creation both metallic (distributed, defragmented) shunts and high-quality ohmic electrodes in magnetic sensing.

1. Introduction

In the last decade, graphene being one of the most important allotrope modification of carbon nanomaterial is widely studied due to its extraordinary physical properties such as high electrical and thermal conductivity, large specific surface area, high mechanical strength and flexibility, etc. as well as future applications. These fascinating properties initiate designing of various graphene-based structures for fabrication of new types of sensors, transducers, spintronic devices, memristors as well as for application in energy storage, magnetic bio-imaging, etc. [1-3].

In particular, a significant part of research is devoted to metal/graphene hybrid structures [4-7], which could be potentially applied in magnetosensorics [7-11]. This application, first of all, needs the formation of high-quality low-ohmic (barrier-free) contacts that do not introduce distortions into the crystal lattice of graphene. However, this point still remains a strong challenge both from fundamental and

technological aspects. Therefore, understanding of mechanisms of the charge carriers' movement near and through the metal/graphene contact area becomes crucial. Carrier transport in such metal/graphene nanostructures depends on many factors, such as the method of graphene synthesis (micro-cleavage, CVD, epitaxy, etc.), the type of graphene (single-layered, multilayered, twisted) and substrate, on which graphene is deposited, as well as the type, concentration and distribution of possible defects in graphene, including those incorporated by polycrystallinity and deposition of metallic clusters [1-3, 11].

Several mechanisms of electric carrier's transport both with and without external magnetic field observed in graphene and metal/graphene structures are generally discussed in literature. Most commonly, carrier transport in pristine graphene is described by the interferential mechanisms considered in the theory of quantum corrections to the Drude conductivity in weak localization conditions [12,13,15-19]. As reported in [19], for graphene produced by mechanical exfoliation this mechanism includes several contributions – low localization taking into account electron-electron interaction [12, 13,16-18], intervalley scattering and chirality breaking [16], weak antilocalization [16,17], etc. The second mechanism of electrical conductivity in graphene is variable range hopping (VRH) of electrons by the localized states considered within the models of Mott [14, 20, 21] and Shklovsky-Efros in zero external magnetic field [22] and within the models of Mikoshiba [23], Shklovsky [22] and Altshuler-Aronov-Khmelnitski [12] for conductivity in non-zero magnetic field. It is worth noticing that hybrid graphene/metal structures containing semiconducting graphene layer with a special metallic shunt and a number of electric contacts could also demonstrate extraordinary magnetoresistive effect (EMR) of geometrical nature observed at high transversal magnetic field when current routes are modified under the Lorentz force [24-30]. This effect originates from structural inhomogeneities (precipitates, surface inclusions, defects and their crowds, etc.) in graphene sheet due to formation of large-scale potential relief (LSPR).

In order to clarify possible mechanisms of electric transport in metal/graphene structures, present paper is focused on the investigation of variation in electrical conductivity and magnetoresistance of the twisted graphene sheets when decorating with Co particles, which can play the role of both metallic (distributed) shunt and high-quality low-ohmic electrodes.

2. Experimental

Sheets of twisted graphene, characterized with in-plane rotation of graphene layers by an angle θ, were fabricated by the method of atmospheric pressure chemical vapor deposition (AP CVD) on 25 μm thick Cu foil (Alfa Aesar 99,8 % purity) from n-decane precursor $C_{10}H_{22}$ with nitrogen as a carrier gas, under experimental conditions previously reported elsewhere [31]. Twisted graphene is chosen as a substrate for deposition of Co nanoparticles because multilayered graphene possesses higher number of conducting channels, higher band overlap and is much less affected with the substrate as compared to single-layered graphene [32,33].

To analyze electrical resistivity of twisted graphene, sheets were transferred from Cu foil onto the dielectric substrates of silicon oxide (SiO_2). The transfer was performed after dissolution of Cu foil in 1 M $FeCl_3$. After this procedure graphene sheets were washed out in distilled water and transferred onto SiO_2/Si substrate (samples *G*/SiO_2).

Electrochemical deposition of Co particles onto the surface of graphene sheet on Cu foil was carried out at a constant current with density 2.5 mA/cm^2 during 30 s at room temperature as it described in [34]. The used electrolyte contained 0.96 g/l of cobalt sulfate and 0.064 g/l of sodium chloride, solved in distilled water. All chemicals were of analytical grade. The obtained samples of graphene sheet on Cu foil with electrochemically deposited Co particles were thoroughly washed with distilled water and dried at room temperature.

To analyze electrical resistivity of twisted graphene and twisted graphene decorated with Co nanoparticles, sheets were transferred from Cu foil onto the dielectric substrates of silicon oxide (SiO_2). The transfer was performed after dissolution of Cu foil in 1 M $FeCl_3$. After this procedure the sheets of graphene and graphene with Co nanoparticles were washed out in distilled water and transferred onto SiO_2/Si substrates (samples *G*/SiO_2 and Co-*G*/SiO_2, respectively).

Surface morphology of *G*/SiO_2 and Co-*G*/SiO_2 samples both on copper foil and SiO_2/Si substrates was examined by scanning electron microscopy (SEM) on Hitachi S4800 device equipped with the Bruker QUANTAX 200 energy dispersive X-ray spectrometer (EDXS) enabling determination of the material elemental composition maps. Quality of graphene layer was also estimated using Raman

spectroscopy (RS) Confotec NR500 confocal micro-Raman spectrometer with 473 nm excitation wavelength and spectral resolution about 3 cm^{-1} [32, 34, 35, 36]. We additionally examined the thickness of graphene transferred on glass by the light transmittance measurement in 400-800 nm wavelength range (PROSCAN MC-121 spectrometer). The value of transmittance > 94% (at 550 nm) allows to conclude the average number of graphene layers equal two.

Four-probe electric resistance as a function of temperature T and magnetic field B applied normally to the surface of G/SiO_2 and Co-G/SiO_2 samples was measured in the closed-cycle refrigerator system (CCRS), produced by Cryogenics Ltd (London), in the temperature range $2 < T < 300$ K and magnetic fields with induction B up to 8 T perpendicular to the electric current. The relative magnetoresistance is defined as $MR = 100\% \times [R(B)-R(0)]/R(0)$, where $R(B)$ and $R(0)$ are resistances at non-zero and zero magnetic fields B, accordingly. Measurements were performed on the samples arranged on the contact pad (Figure 1a), using 4 indium (In) supersonically soldered electric contacts with soldered 50 μm diameter copper wires. Measurement cell with a sample on the contact pad was placed in a special measuring probe included LakeShore thermometers and magnetic field sensors, heaters, heated thermal shields, all in He gas atmosphere under low pressure. The probe was inserted into channel of superconducting solenoid inside the cryostat in CCRS. Temperature was stabilized with the precision not less than 0.01 K using LakeShore 331 measuring controller.

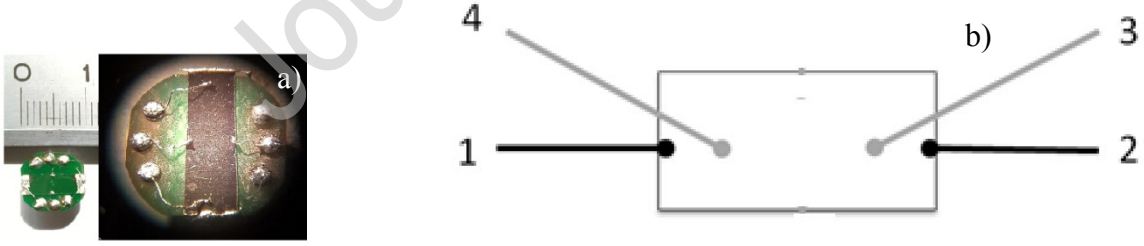

Fig. 1. The photo of sample on contact pad (a) and scheme of electric probes arrangement (b) where 1, 2 are current contacts; 3, 4 are potential contacts

In present study $R(T)$ curves were re-calculated into either surface resistance

$$R_{\square}(T) = R(T) \times (W/L)\ [\Omega/\square] \quad (1)$$

or into resistivity

$\rho(T) = R(T) \times (W \times d/L)$ [Ω×m] (1b)

or conductivity

$\sigma(T) = (1/\rho(T))$ [Sm/m], (1c)

where W is the width of current conductive channel (of the graphene layer), d is thickness of the graphene layer, L is distance between potential contacts 3 and 4 in Figure 1b. The error in $\rho(T)$ measurement was mainly limited by the size of electric contacts and intercontact distances and was equal or less than 5 %.

3. Structure of the samples before and after Co particles deposition

Typical SEM image of Co-G/SiO_2 is presented in Figure 2. It is seen that the mean diameter $\langle d \rangle$ of Co particles equals to 220 nm. Deconvolution of experimental high-resolution Co core level X-ray photoelectron spectra recorded on Co-G/SiO_2 is considered in the paper [34]. It is indicated that metallic particles possess Co "core"/Co oxide "shell" structure.

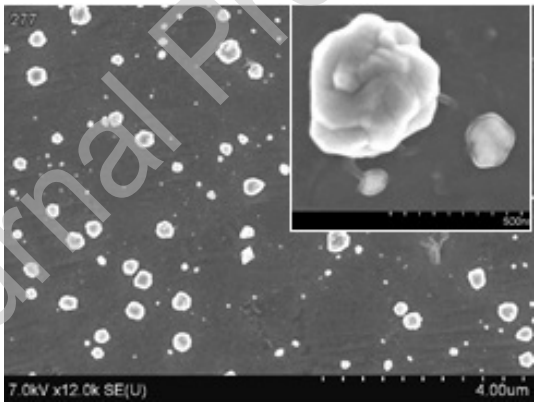

Fig. 2. Scanning electron microscope (SEM) image of Co-G/SiO_2 sample. The inset shows SEM image at higher magnification.

The typical Raman spectra of the G/SiO_2 and Co-G/SiO_2 samples are presented in Figures 3a and b, correspondingly. One may see that D peak is more intense for the sample decorated with Co nanoparticles. Indeed, the I_G/I_D ratio distributions, recorded over the 20x20 μm^2 area for each sample,

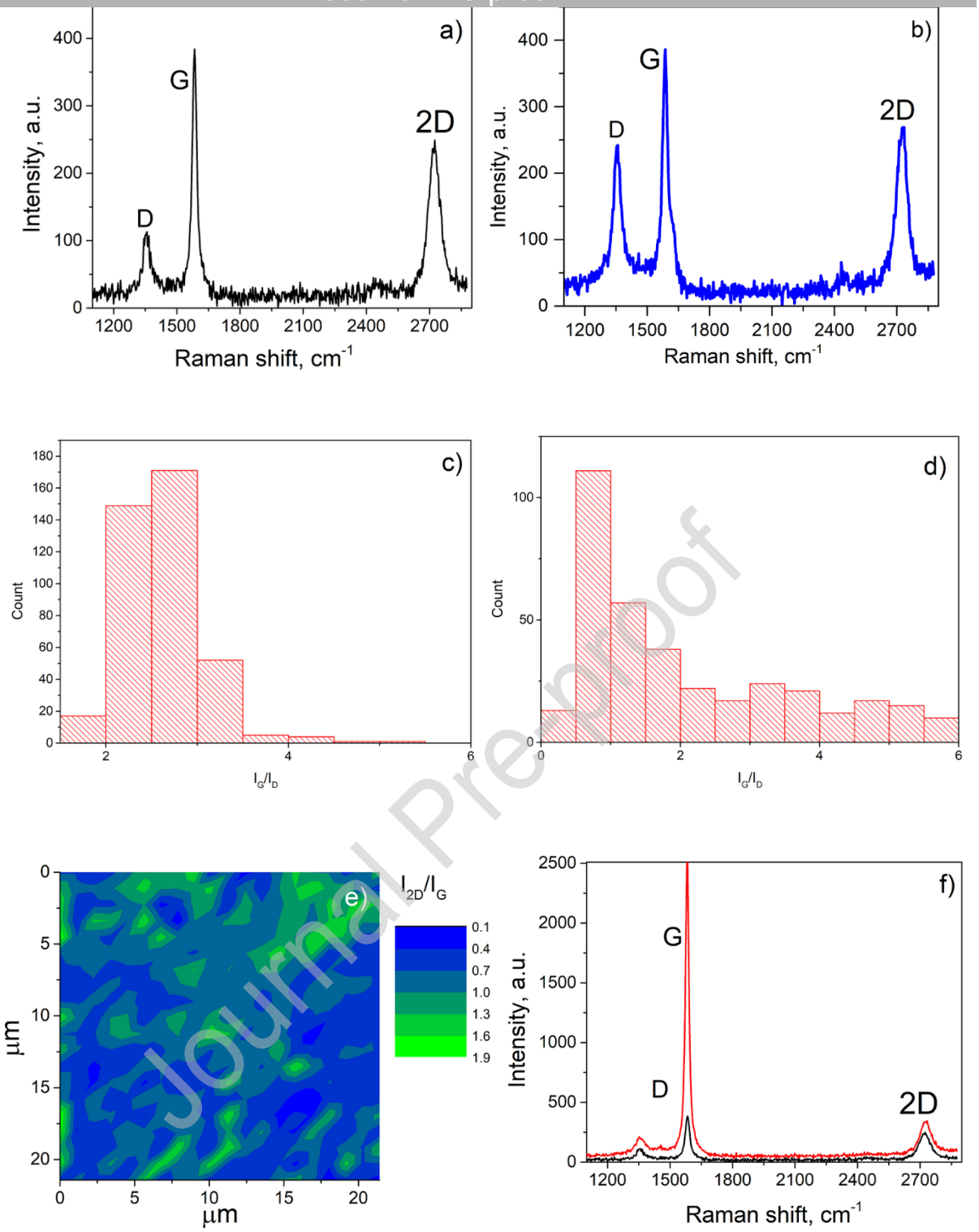

Fig. 3. Raman spectra (a, b) and histograms I_G/I_D ratios (c, d) for G/SiO_2 (a, c) and Co-G/SiO_2 (b, d) samples; the mapping of I_G/I_D ratios for Co-G/SiO_2 sample (e); comparison of two Raman spectra recorded from different places of G/SiO_2 sample (f)

plotted in Figures 3c and d, for G/SiO_2 and Co-G/SiO_2 samples, respectively, reveal noticeably higher defectiveness for Co decorated sample. This result is in contrast with our earlier report [34] where no

significant impact of Co deposition on graphene structure laying on copper foil were noticed. This sort of discrepancy can be explained by the following arguments. In present paper, Co was deposited directly on graphene on copper foil, only after that Co-*G* structure was transferred onto SiO_2 surface by the wet transfer method. Most likely, nanoparticles decoration changes the surface energy of graphene which affects its wettability [37]. Since, no polymeric carcass was used for the transfer, the stress in graphene caused by non-optimal tension of etchant liquid on graphene may lead to the formation of wrinkles and increasing of *D* band intensity in Raman spectra, which was observed in our earlier experiments [34, 38].

Raman spectroscopy also allows evaluation of electronic structure of graphene. Mapping of I_{2D}/I_G ratio for Co-*G*/SiO_2 sample presented in Figure 3e reveals that twisted graphene used in our study was inhomogeneous. It was reported previously that different values of I_{2D} observed in twisted graphene are related to its parts with different twisted angles [31]. The most pronounced manifestation of twisted nature of graphene is the significant increasing of *G* band intensity (*G*-resonance [39]) in Raman spectra when the energy of excitation light quantum fits to the energy difference between singularities in density of states (van Hove singularities). This is illustrated in Figure 3f, which shows two Raman spectra recorded from different parts of *G*/SiO_2 sample where the excitation energy does and does not satisfied above described condition. The domain size of uniform electronic state estimated from the areas of the I_{2D}/I_G appears to be in the range of few μm. Therefore, since the angle θ defines electronic properties of twisted graphene [39], one can conclude that *G*/SiO_2 and Co-*G*/SiO_2 samples possess polycrystalline structure, where each domain represents an area with distinct electronic properties.

4. Electrical resistance of *G*/SiO_2 and Co-*G*/SiO_2 samples

Experimental dependencies of $R_{\square}(T)$ and their normalized values $R_{\square}(T)/R_{\square}$(300 K) are plotted in Figures 4. As follows from Figure 4a, $R_{\square}(T)$ curves near the room temperatures are characterized by negative value of the resistance temperature coefficient, thus evidencing the influence of activational mechanism of carrier transport in our samples. This should be assigned to the polycrystalline structure and quite high density of defects in the twisted graphene as was considered in [40-45]. Semiconducting

(activational) behavior of G/SiO_2 and Co-G/SiO_2 samples around 300 K is proved by normalized $R_{\square}(T)/R_{\square}(300\ K)$ curves plotted in the Arrhenius scale (Figure 4b). We can distinguish on these curves high-temperature linear sections with slopes denoting activation energy of conductance activation E_{σ}. The estimated values of E_{σ} around room temperature were 5,9 meV and 15,5 meV for G/SiO_2 and Co-G/SiO_2, correspondingly. Moreover, at temperatures T around 273 K (room temperature) values of $R_{\square}$ are almost independent on T, which is characteristic for semiconductors within impurities depletion area, when $R_{\square}(T)$ is defined only by carriers mobility. Comparison of Figures 4a and 4b shows that decoration of graphene with Co particles results in the decrease of $R_{\square}$ values up to several times, which can be attributed to the change of mechanisms of carrier scattering.

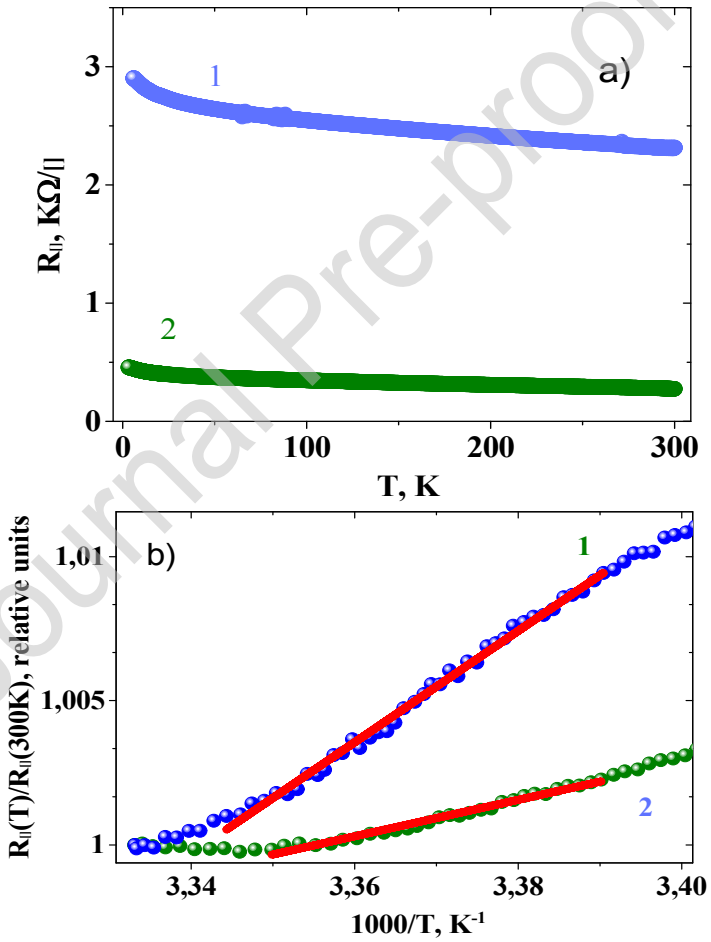

Fig. 4. Temperature dependencies of surface electrical resistance $R_{\square}(T)$ for the samples G/SiO_2 (1) and Co-G/SiO_2 (2): (a) normal scale; (b) Arrhenius normalized dependencies $R_{\square}(T)/R_{\square}(300\ K)$ *vs* $_{\square}(1000/T)$. Linear parts of the curves $\ln(R_{\square}(T)/R_{\square}(300\ K))$ -(1000/T) (approximated with solid lines) correspond to activational law for carrier transport.

The $R_{\square}(T)$ curves for both types of samples plotted in Arrhenius scale reveal that at low temperatures (below 200 K) they are characterized by variable activational energy with temperature decrease. There are two main reasons for such behavior of G/SiO_2 and Co-G/SiO_2 structures at low temperatures: either variable range hopping (VRH) conductance by the localized states near Fermi level [14,20,21] or quantum interference corrections to the Droude conductivity in conditions of weal localization [12,13,15-19]. Note, that in VRH regime temperature dependencies of electrical conductivity can follow the Mott-like expressions

$$\sigma_{\square}(T) \approx \sigma_{02}\exp\left[-\left(\frac{T_0^{2D}}{T}\right)^{0,33}\right] \quad (2)$$

where σ_{o2}, T_o^{2D} are characteristic parameters for Mott (with α= 0.33 for 2D [14]) or Shklovsky-Efros (α= 0.5 [20]) VRH models, correspondingly. These parameters define the probability of carriers hopping and the energy of their activation (or hopping length) [14, 21]. It is well established, that the experimental values of both T_o^{2D} have to exceed the temperature of measurements because otherwise, the values of activation energy for VRH mechanism is below the energy of phonons, which has no physical meaning. To estimate characteristic parameters in Eqs. (2), we used fitting procedure by the method of least squares.

As was mentioned in Introduction, in accordance with theories [12,13,15-19], temperature dependences of quantum corrections (QC) $\Delta\sigma_{QC}^{D}(T)$ to the Droude conductivity also depend on dimensions of samples D, following equation for weak localization in 2D samples

$$\Delta\sigma_{QC}^{2D}(T) \sim \pm\frac{e^2}{\pi h}\ln(\tau T) \quad (3)$$

for weak localization in 2D case, where τ are times of phase breaking due to elastic or quasi-elastic scattering of electrons on defects, impurities, etc. and also at taking into account electron-electron scattering, if needed [12,13,15]. To separate contributions (2) or (3) into carrier transport, we should represent $\sigma_{\square}(T)$ in different coordinates. For example, Figure 4b shows the temperature dependencies of the electrical sheet conductance $\sigma(T)$ at 2 < T < 25 K in Mott scale for 2D VRH mechanism (a) and in semi-logarithmic coordinates for extraction of QC contributions (b).

Linearization of experimental $\sigma_{\square}(T)$ dependences in Mott coordinates for 2D case in temperature range 10 < T < 20 K (Fig. 5a) confirms the presence of Mott-like sheet conductance in the studied samples. Linearization of semi-logarithmic curves $\sigma_{\square}(T)$-lg$T$ in Figure 5b below 10-15 K (where Mott VRH contribution is negligible) confirms the presence of contribution of quantum corrections to Droude conductivity in this temperature range. Saturation of these curves at T < 5 K can be attributed to the tendency of $\sigma_{\square}(T)$ towards minimal metallic conductivity σ_{min} when approaching the metal-insulator transition in disordered crystals [20, 21].

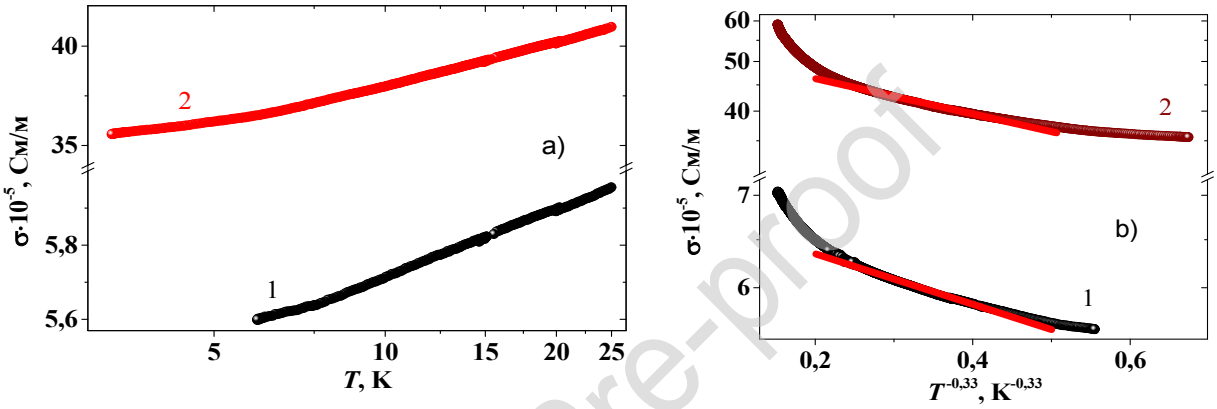

Fig. 5. Temperature dependencies of sheet conductance $\sigma(T)$ below 25 K for G/SiO_2 (1) and Co-G/SiO_2 (2) in semilogarithmic scale appropriated to quantum corrections (a) and in Mott scale for 2D VRH (b)

The assumption on the role of QCs in low-temperature carrier transport is also follows from the temperature dependencies of the breaking phase time τ_φ estimated from the well-known expression [13, 46, 48]

$$\left(\frac{\hbar}{\tau_\varphi}\right) = kTG_0R_{\square}Ln\left(\frac{1}{\pi G_0 R_{\square}}\right), \quad (4)$$

where $G_0 = e^2/2\pi^2\hbar = 1.23\cdot10^{-5}$ Ohm^{-1} and $R_{\square} = (1/\sigma_{\square})$. According to quantum corrections theory [12,15], shape of the $\tau_\varphi(T)$ curves should follow the power dependence

$$\tau_\varphi(T) \sim T^{-p}, \quad (5)$$

where parameter p is defined by the mechanism of wave function phase breaking lying within the range $1 < p < 2$ [15]. The estimated $\tau_\varphi(T)$ dependencies shown in Figure 6 clearly evidence the power-like

$\tau_\varphi(T)$ curves. Values of p estimated from the slopes of the straight lines in Figure 6 are 0.97 and 0.94 for the samples G/SiO_2 and Co-G/SiO_2 accordingly, that well corresponds to the results of other papers [12, 13, 16-18].

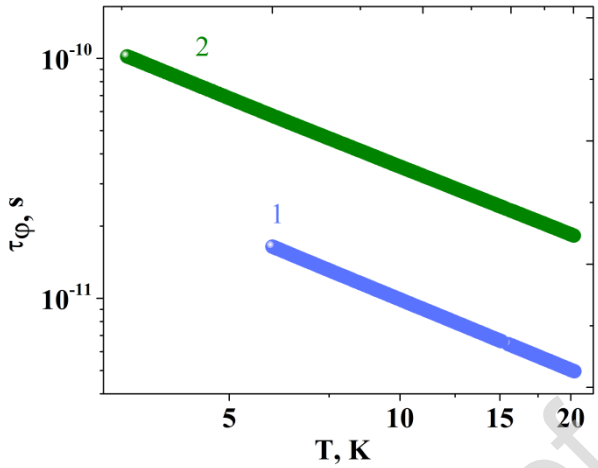

Fig. 6. Temperature dependencies of the phase breaking time $\tau_\varphi(T)$ plotted in logarithmic scale in the temperature range 2 - 20 K for G/SiO_2 (1) and Co-G/SiO_2 (2) samples.

Thus, the performed analysis of the $\sigma_\square(T)$ dependencies at $2 < T < 25$ K clearly reveals that two possible contributions to the carrier transport mechanisms coexist in twisted graphene: (a) the 2D Mott VRH [14, 20,21] and (b) 2D quantum corrections mechanism [12, 13, 16]. In order to verify this result, we measured the dependencies of electrical sheet resistance $R_\square$ and relative magnetoresistance MR on external magnetic field with induction B to analyze experimental curves in accordance with various models of hopping conductance and QCs in magnetic fields. The $R_\square(B)$ and $MR(B)$ dependencies for G/SiO_2 and Co-G/SiO_2 are presented in Figures 7 and 8, respectively.

Firstly, Figure 7 and 8 show that at low temperatures $R_\square(B)$ and $MR(B)$ curves obtained for both samples reveals competition of negative (NMR) and positive (PMR) contributions to magneto transport. The second peculiarity is that below 50 K NMR contribution prevails only in magnetic fields below 1-2 T, and this contribution decreases after the deposition of Co particles (compare Figures 8a and 8b as well as Figures 9a and 9b).

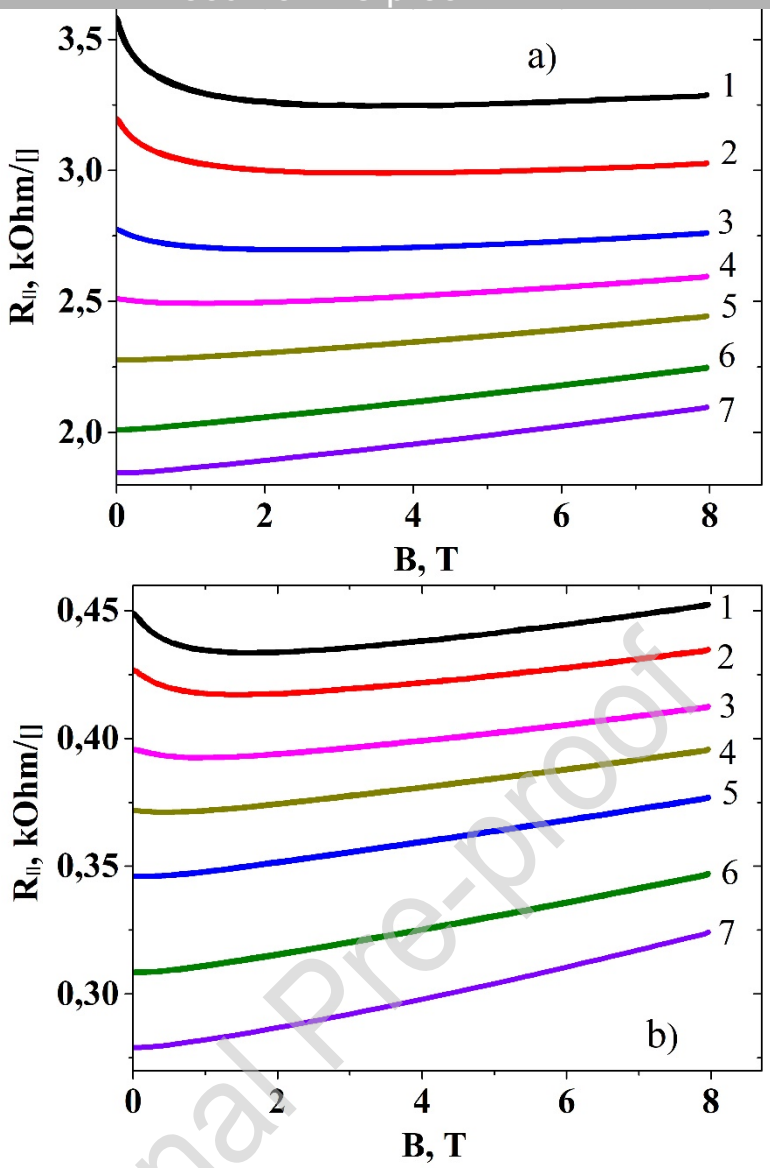

Fig. 7. The dependencies of electrical sheet resistance $R_{\square}$ on applied magnetic field B for G/SiO_2 (a) and Co-G/SiO_2 (b) samples at temperatures T = 5 K (1), 10 K (2), 25 K (3), 50 K (4), 100 K (5), 200 K (6), 300 K (7)

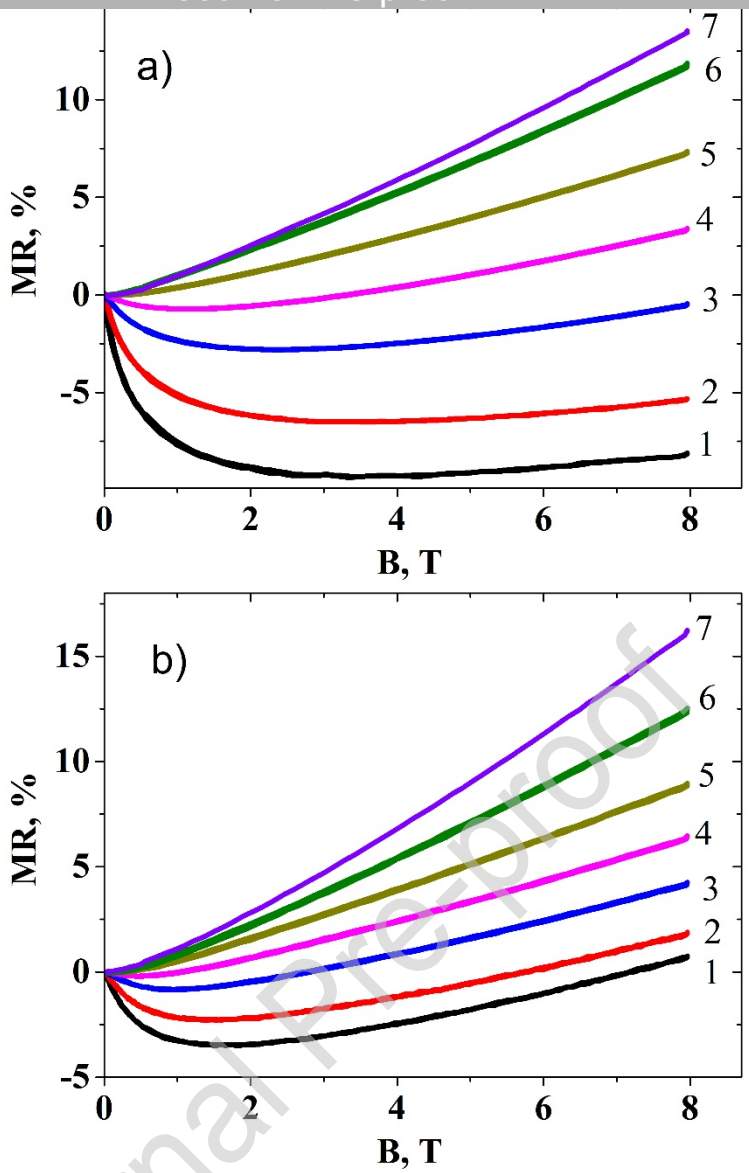

Fig. 8. The dependencies of *MR* on applied magnetic field *B* for G/SiO_2 (a) and Co-G/SiO_2 (b) samples at temperatures *T* = 5 K (1), 10 K (2), 25 K (3), 50 K (4), 100 K (5), 200 K (6), 300 K (7).

It is worth mentioning that contribution of PMR into $R_{\square}(B)$ and $MR(B)$ increases with the growth of both magnetic induction *B* (Figures 9) and temperature (Figures 7 and 8), so that at $T > 100$-120 K we could observe only PMR contribution. Finally, Co-G/SiO_2 samples demonstrate larger *MR* in PMR contribution with close to linear shape of $R_{\square}(B)$ curves at $B > 5$ T. In so doing, $MR(B)$ curves for Co-G/SiO_2 samples (Fig. 8b) are going much steeper with respect to the G/SiO_2 samples.

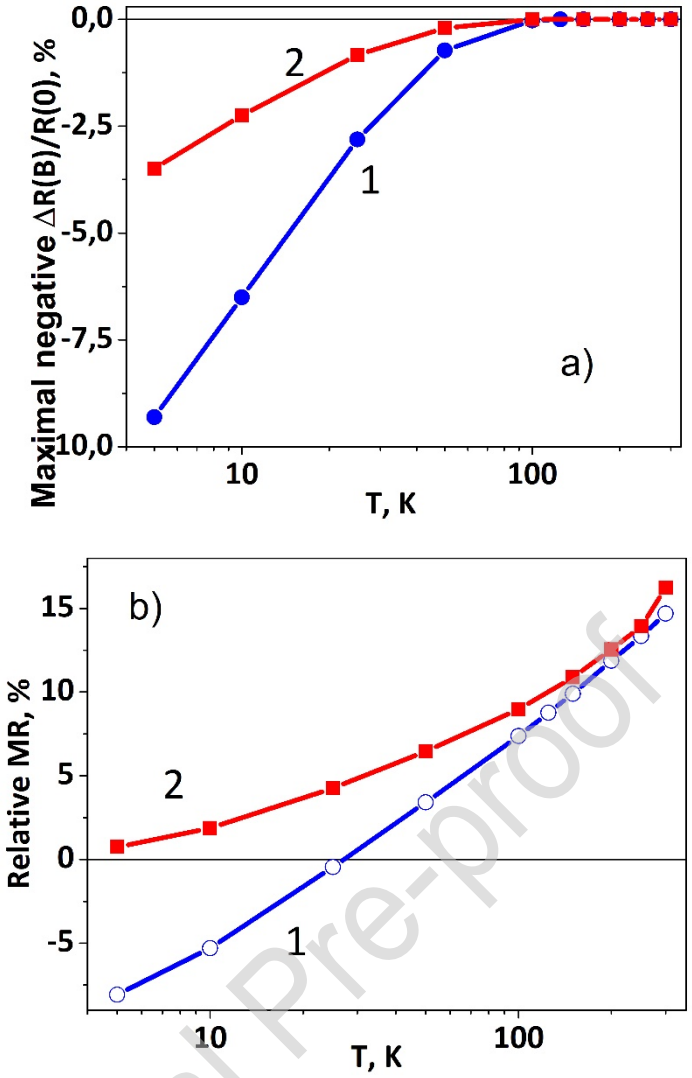

Fig. 9. Temperature dependences of maximal NMR effect (a) and relative *MR* (b) achieved at B = 8 T for G/SiO_2 (1) and Co-G/SiO_2 (2).

Concerning observation of low-temperature NMR contribution in graphene-based samples, we can state its suppression both with increasing temperature and also after deposition of cobalt particles (compare curves 1 and 2 in Figures 9).

It is typical that in B < 1-2 T NMR contribution can be explained by two main mechanisms: quantum corrections to Drude conductivity in the conditions of weak localization [12,13,15,18] and VRH conductivity [13]. In the last case, $R_{\square}(B)$ dependences at low temperatures are described with the expression introduced by Altshuler-Aronov-Khmelnitski [13]

$$R_{\square}(B) = - R_{\square}(0)\exp(\gamma/B^m), \quad (6)$$

where constant γ depends on the type of defects and localization radii of wave functions for charge carries: in the theory, exponent m equals to 1 or 2 at strong or weak applied magnetic fields B, correspondingly.

For the case of PMR at high B values, the $R_{\square}(B)$ curves at low temperatures are usually considered within the Mikoshiba [23] or Shklovsky [22] models of VRH carrier transport which follow the relationship

$$R_{\square}(B) = + R_{\square}(0)\exp(\beta/B^n). \quad (7)$$

Here constant β is also governed with the defects type of the object and localization radii of wave functions for charge carries, however, contrary to m in the relationship (6), n values in these models are equal to 2 or 1 at weak or strong magnetic fields, correspondingly.

To analyze the PMR effect within Mikoshiba model (7), we plot the $R_{\square}(B)$ dependencies in double logarithmic coordinates $\mathrm{Ln}[\mathrm{Ln}(R_{\square}(B)/R_{\square}(0))] - \mathrm{Ln}B$ presented in Figure 10.

It is seen from Figure 10a, that for the sample G/SiO_2 linearization of $R_{\square}(B)$ in Mikoshiba coordinates in magnetic fields B > 6-7 T is fulfilled only at $T \leq 10$ K where the exponent n, estimated from the slopes of experimental curves, are less than 1. At the same time, as seen from Figure 10b, decoration of graphene with Co particles results in linearization of curves only at T = 25 K where the slope of the experimental curve 3 is close to $n \approx 2$. With the lowering of temperature, the estimated n values have no physical meaning. Hence, we can conclude that Mikoshiba model (7) does not work in the PMR region. This correlates with small contribution of PMR effect in $R_{\square}(B)$ curves in Figure 7a at $T \leq 50$ K.

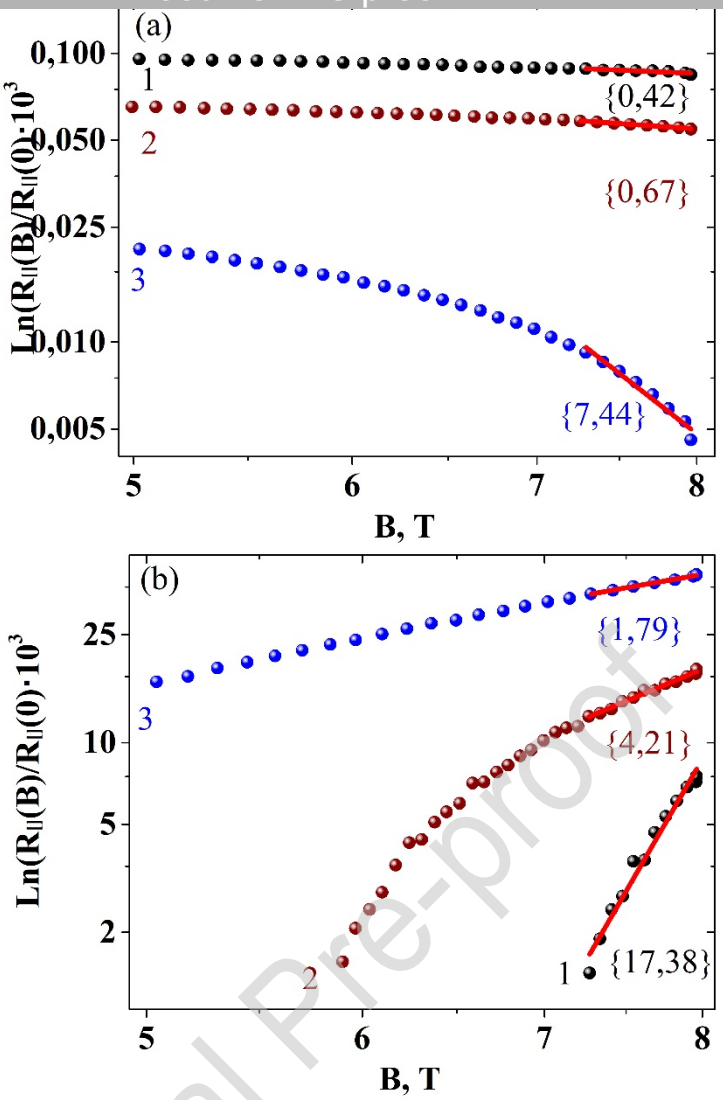

Fig. 10. Typical dependencies of $MR(B)$ at high magnetic fields B (PMR) plotted in Mikoshiba coordinates Ln[Ln($R_{\square}(B)/R_{\square}(0)$)] – Ln($B$) for G/SiO_2 (a) and Co-G/SiO_2 (b) at the temperatures T = 5 K (1), 10 K (2) and 25 K (3). The exponent values n in the Eq. (6) obtained from fitting of experimental curves (dots) with linear functions (red lines) are shown near every curve.

Possible contribution of hopping magnetotransport into NMR was analyzed using the expression (6) accordingly to Shklovsky-Altshuler-Aronov-Khmelnitski model [12]. As presented in Figure 11, estimation of m values, in accordance with the scheme described above for the analysis of PMR effect, exhibits that at weak magnetic fields (below 1 T) and 5 < T < 25 K behavior of Ln[Ln($R_{\square}(B)/R_{\square}(0)$)] – Ln$B$ curves is very close to linear with m ~ 1 for both G/SiO_2 and Co-G/SiO_2 samples. However, the increase of applied magnetic field above 0.8 – 1.0 T results in strong discrepancy between experimental

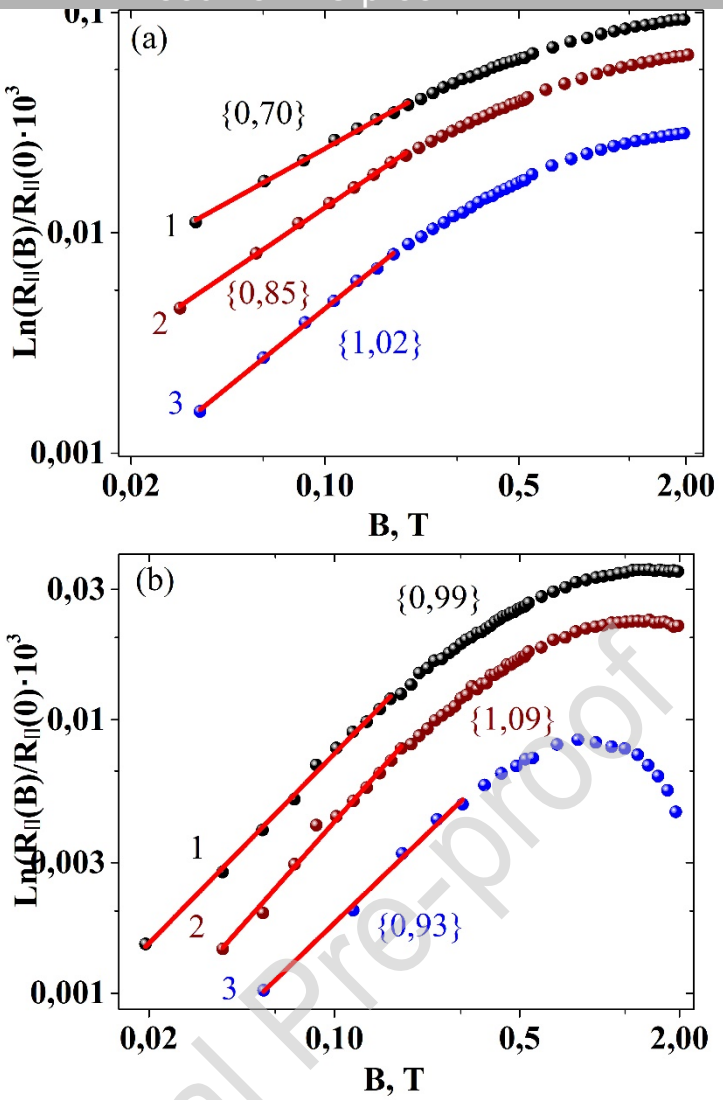

Fig. 11. Typical dependencies of $MR(B)$ at low magnetic fields B (NMR) plotted in Mikoshiba coordinates $\mathrm{Ln}[\mathrm{Ln}(R_{\square}(B)/R_{\square}(0))] - \mathrm{Ln}(B)$ for G/SiO_2 (a) and Co-G/SiO_2 (b) at the temperatures T = 5 K (1), 10 K (2) and 25 K (3). The exponent values n in the Eq. (5) obtained from fitting of experimental curves (dots) with linear functions (red lines) are shown near every curve.

points and model Altshuler-Aronov-Khmelnitski (6). This means that hopping contribution into NMR in accordance with model (6) [13] is rather likely suppressed with the temperature increase.

5. Discussion

Let us discuss the reasons of the observed influence of twisted graphene decoration with Co particles on the values of sheet resistance $R_{\square}$ and its dependence on temperature and magnetic field.

As follows from Raman spectroscopy and SEM experiments, the deposition of Co particles on twisted graphene sheet enhances defective structure of the sample Co-G/SiO_2 as compared to pristine G/SiO_2. At the same time, as follows from comparison of curves 1 and 2 in Figures 4 and 5, we can observe evident decrease of the sheet resistance after the deposition of Co particles. This testifies the formation of a good electric contact (without existing any barriers) between Co particles and graphene layer. Therefore, metallic clusters, probably causing new defects, act as shunts which short-circuiting grain boundary barriers being in pristine polycrystalline graphene layer under them. The other role of Co particles deposition can be strong change in phase coherence length of carriers when they cross the interface between graphene and Co particles.

The observed differences in experimental temperature dependencies of $MR(B)$ for G/SiO_2 and Co-G/SiO_2 samples reveal the noticeable effect of Co particles decoration on the relation between NMR and PMR contributions. In order to elucidate this role of Co particles decoration, we should estimate quantitatively the relative change under the impact of decoration into temperature dependences of normalized sheet resistance $[R_G(T) - R_{Co\text{-}G}(T)]/R_G(T)$ plotted at definite values of magnetic field B. Such curves are presented separately for the NMR (Figure 12a) and the PMR (Figure 12b).

It is seen that the linearization of the normalized $[R_G(T) - R_{Co\text{-}G}(T)]/R_G(T)$ dependencies in semilogarithmic scale in the range of low T is observed both for the areas where dominates NMR (Figure 12a) as well as where PMR is observed (Figure 12b). The difference is only in the slopes of the linearized dependencies which decreases with the increase of B values for NMR (Figure 12a) and remains almost constant for the area where PMR prevails (see Figure 12b). Such a behavior means that in the area of NMR the relative decrease of the sheet resistivity at low T values becomes two times higher in Co-G/SiO_2. At the same time at $2 < T < 25$ K in the area of PMR the relative contribution of Co decoration into the resistance is practically independent on temperature.

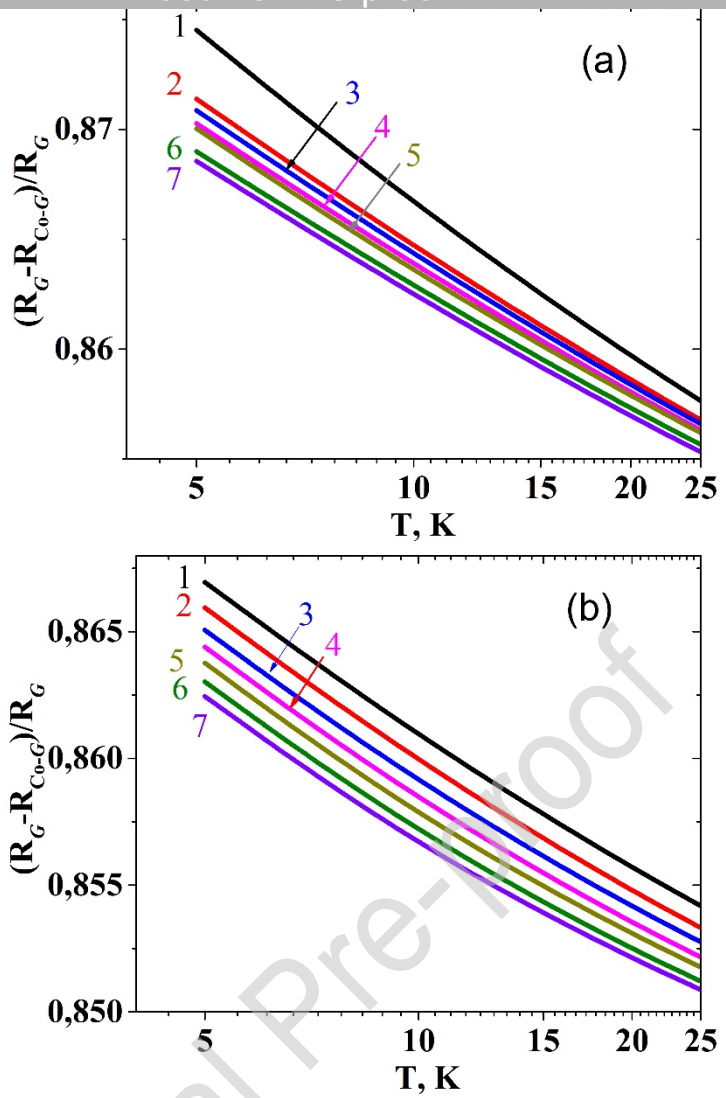

Fig. 12. Temperature dependencies of $[R_G(T) - R_{Co\text{-}G}(T)]/R_G(T)$ in the area of NMR (a) and PMR (b) for low temperatures plotted in semilogarithmic scales. For NMR area, values of applied magnetic fields B are: 1-0 T, 2-0.2 T, 3-0.3 T, 4-0.4 T, 5-0.5 T, 6-0.750 T and 7-1.0 T. For PMR region values of B are: 1-2 T, 2-3 T, 3-4 T, 4-5 T, 5-6 T, 6-7 T and 7-8 T.

It is worth noticing that observed linearization of low-temperature $[R_G(T) - R_{Co\text{-}G}(T)]/R_G(T)]$ semi-logarithmic curves in the NMR area indirectly confirms the role of contribution of quantum corrections into the electrical conductivity in weak magnetic fields and at temperatures lower than 10 K.

At the same time, decoration of graphene with Co particles results in the increase of VHR conductivity in the NMR contribution. This is evidenced from the linearization of $[R_G(T) - R_{Co\text{-}G}(T)]/R_G(T)$ curves in Mott scale for 2D case in the range of T = 10-25 K which is shown on Figure 13. The observed

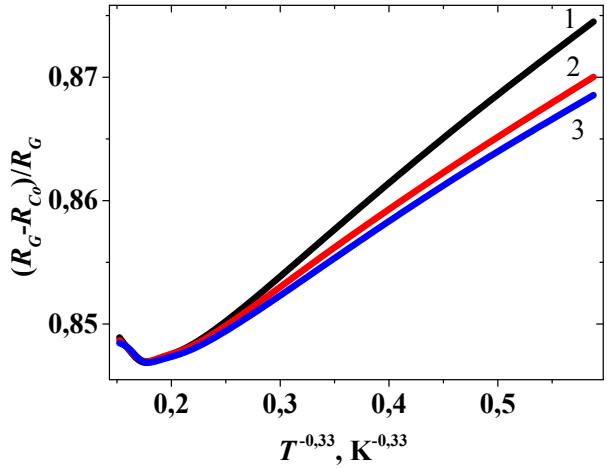

Fig. 13. Temperature dependencies of relative increment of magnetoresistance $[R_G(T) - R_{Co\text{-}G}(T)]/R_G(T)$ in the range of NMR due to deposition of Co on graphene, plotted in 2D Mott scale for low temperatures and low magnetic fields B = 0 T (1), 0,5 T (2) and 1,0 T (3)

change of the slopes of the linearized parts of the curves in Figure 13 reveals that parameter T_o in the relationship (3) depends on the magnetic field B, possibly either due to the compression of the wave functions [14,22] or due to influence of B on characteristic temperature T_o (which determines the probability of electron jump) in Eq. (2) in accordance with Altshuler-Aronov-Khmelnitski model [13]. All this also correlates with the behavior of $MR(B)$ discussed in previous chapter in the frame of the model (6) [13] for low magnetic fields (see, Figure 11).

Effect of Co deposition on $MR(B)$ dependence in graphene can be also analyzed within the frame of a Kohler rule [49] for Lorentz mechanism of MR, which is due to deviation of electron trajectories with respect to the vector of electric field intensity under impact of Lorentz force in perpendicular magnetic field. However, taking into account the linear progress of $MR(B)$ at high B values in Figure 7 and in [26,27,50-53], we have transformed the Kohler rule for highly defected samples into the equation

$$\frac{\rho(\mathrm{B,T})}{\rho(0,\mathrm{T})} = \frac{r}{ne}\left[\frac{B}{\rho(0,\mathrm{T})}\right], \qquad (8)$$

basing on consideration of dimensionality. Here $\rho(0,T)$ is resistivity at temperature T and magnetic induction B = 0 T, e – charge of electron, n – concentration of charge carriers and coefficient r depends on the mechanism of electron scattering. The Eq. (8) allows to calculate concentration of charge carriers $n(T)$,

which is presented in Fig. 14a. The estimated $n(T)$ was used for estimation of mobility of charge carriers $\mu(T)$ presented in Figure 14b using equation

$$\mu(T) = \frac{r}{\rho(T)ne} \tag{9}$$

in the assumption of $r \approx 1$. Here electrical resistivity $\rho(T)$ was calculated from the full resistance R by the Eq. (1b), where we used the thickness d of the twisted graphene as 2.0 of the single-layer graphene thick (0.246 nm).

Figure 14 reveals that calculated n and μ values increase after deposition of Co on graphene sheet. In doing so, curves $n(T)$ dependencies are very weak and possess maximum at T = 10-20 K, while $\mu(T)$ goes through minimum at $T \approx 10$ K (see Figure 14).

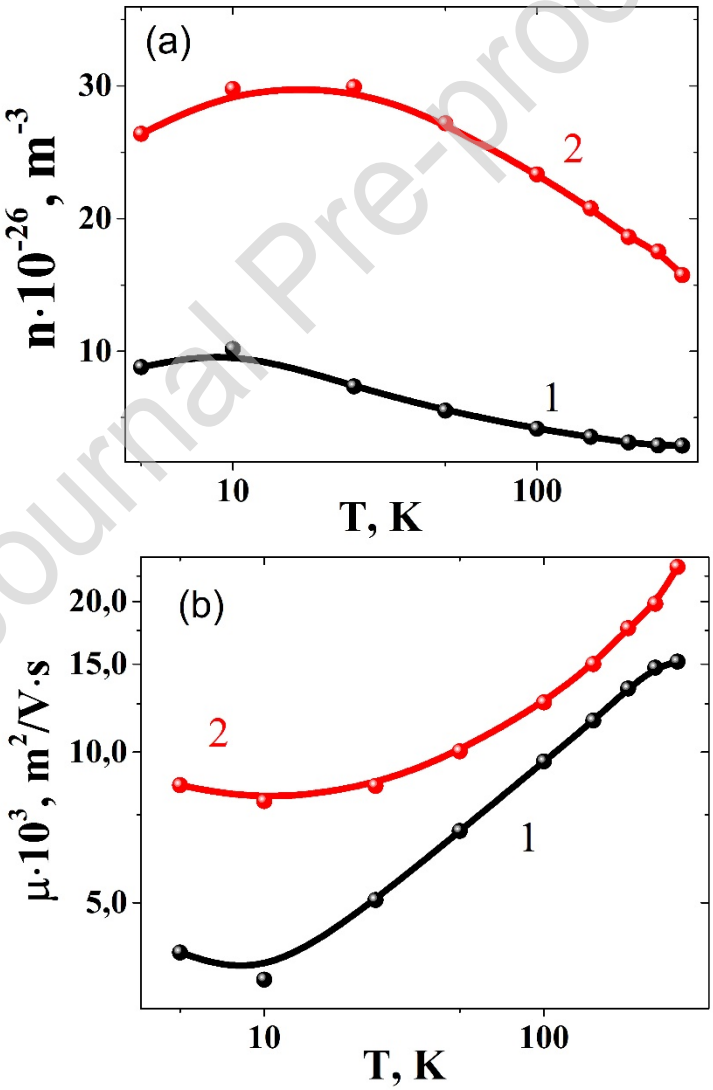

Fig. 14. Temperature dependencies of concentration n (a) and mobility μ (b) of charge carriers in G/SiO_2 (1) and Co-G/SiO_2 (2) samples

Note also that the n values extracted from the transformed Kohler rule (8) agree well with its estimations from Raman spectra [31, 34], which give sheet values of the order of 10^{16} m^{-2} that is close to the bulk values in Figure 14.

Analyzing the calculated $n(T)$ and $\mu(T)$ dependences, we can conclude that combination of high n values together with very low ρ and μ values could be associated with high concentration of defects in the studied samples due to possible formation of large-scale potential relief [20, 21, 50-53]. The reasons for LSPR formation could be the grain boundaries as well as the other types of inhomogeneously distributed defects accumulated in G/SiO_2 and Co-G/SiO_2 sample. This is indirectly confirmed by non-linear character of I-V characteristics at low temperatures, impossibility to measure Hall effect even at high magnetic fields and linear dependencies of $MR(B)$ at high magnetic fields. Our assumption about the formation of LSPR in G/SiO_2 and especially in Co-G/SiO_2 samples well correlates with the results published in [46].

Besides, evaluation of $n(T)$ and μ(T) reveals their increase up to 3 times in Co-G/SiO_2 sample with respect to pristine G/SiO_2 sample, which explains the decrease of electrical resistance of graphene decorated with Co particles. Possible reasons for that will be considered below in detail.

Remind that parameters p in (4) are close to 1 in Fig. 6. This means that most probable phase breaking mechanism for G/SiO_2 and Co-G/SiO_2 samples is electron-electron scattering in weak localization conditions [16-18]. Considering the values of $\mu(T)$ in Fig. 14b, we can estimate the values of transport time of momentum relaxation from the known relation $\tau_{tr} \approx [m^*\mu(T)/e$ and calculate the values of parameters of electron-electron scattering K_{ee} from the slopes of curves in Figure 15 using the equation

$$\Delta\sigma_{ee} = K_{ee}G_o\mathrm{Ln}(kT\tau_{tr}/h). \quad (10)$$

The estimated values are 1.7 nm^{-1} for G/SiO_2 and 25.3 nm^{-1} for Co-G/SiO_2 samples that is very close to theoretical predictions in [12, 49].

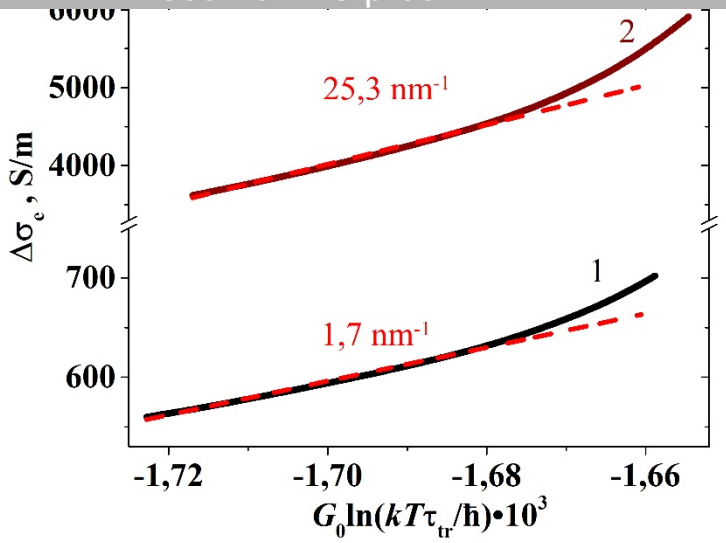

Fig. 15. Temperature dependences of quantum correction $\Delta\sigma_{ee}$ calculated from curves in Figure 5b in coordinates of Eq. (10) [12, 46].

As evidenced from the above analysis of experimental data, one should note the drastic difference in the behavior of *MR*(*B*) at temperatures below 50 K for *G*/SiO_2 and Co-*G*/SiO_2 samples. In particular, NMR effect in *G*/SiO_2 sample dominates only at $B < 1$ T and essentially (up to 2 times) decreases after the deposition of Co particles (in Co-*G*/SiO_2 sample). Remind also, that deposition of Co particles enhances the PMR effect, so that *MR*(*B*) curves in Co-*G*/SiO_2 sample go much steeper that for the pristine *G*/SiO_2 (compare, Figures 7 and 8). We consider the mentioned differences of *MR*(*B*) curves in *G*/SiO_2 and Co-*G*/SiO_2 as development of EMR effect [24-30, 54, 55] within the proposed phenomenological model presented in Figure 16.

Our model is based on the approach described in [54] and modified in [55] for the case of composite metal-semiconductor structures, where *a single* round metallic inclusion was embedded into a semiconductor. Rowe and Solin [54] showed by solving the Laplace equation that external impacts (for example, magnetic field, mechanical stresses, etc.) can lead to significant changes in the distribution of electrical resistance *R* over such a structure. As a result, at certain ratio between properties of the metal inclusion and semiconductor film, as well as the contact resistance between them, the change in full resistance in such a composite structure can be much larger in magnitude than observed in pure semiconductor (without metallic inclusion). For example, according to [54, 55], in such structures the

application of a magnetic field B perpendicular to the plane of the semiconductor may cause the EMR effect. Such behavior of $MR(B)$ indicates that for some values of B the magnitude of the magnetoresistive effect in the composite metal-semiconductor structure (at least in some places) will differ significantly from those for pure metal and pure semiconductor. In general, as follows from [54, 55], in order to enhance the impact of the magnetic field on magnetoresistance, it is necessary to make such a composite where the electron trajectories (current routes) at the metal-semiconductor interface are maximally changed. This is especially true for the case of several metallic particles distributed over the surface of graphene sheet presented in Fig. 16.

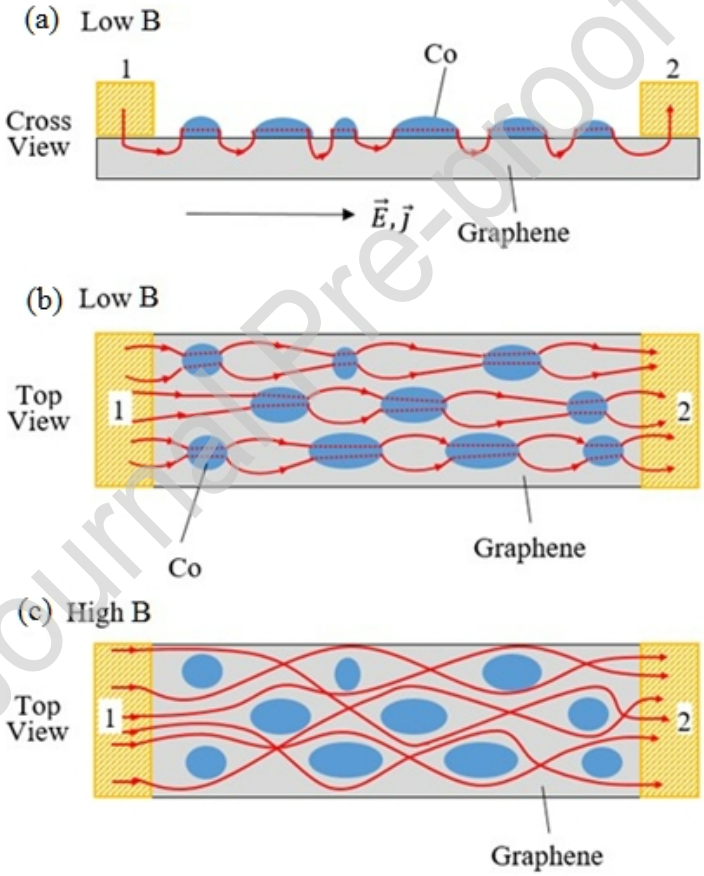

Fig. 16. Scheme of current routes (red lines with arrows) in Co-G/SiO_2 sample: cross-section (a) and top views for low (b) and high (c) magnetic field B. The grey area is a graphene layer, yellow stripes are electric contacts 1 and 2, blue spots are Co particles. Vector B is normal to graphene layer plane.

Basing on this approach, the scheme in Figure 16 illustrates possible changes of current conducting routes in graphene (which replaces the semiconductor in the model [54, 55]), with multiple Co particles randomly distributed over its surface. According to [55], at low magnetic fields B, the current is concentrated in the metallic region (cobalt particles), lying on graphene sheet and acting as a short circuits (shunts) due to their low-ohmic contact with graphene (see dashed lines crossing Co clusters in Figures 16a and 16b). In this case, in accordance with our model, current routes and the current density vector $\boldsymbol{j}$ are parallel to the total electric field $\boldsymbol{E}$, so that resistance changes weakly under magnetic field (the lengths of current routes are almost unchanged when B growing). So, the cobalt particles on graphene sheet looks like equipotential bodies due to their high conductance.

In contrast, at high magnetic fields B, the current lines near metallic particles (Figure 16c) are strongly deflected from their homogeneous distribution by Lorentz force [54]. This results in a directional difference between $\boldsymbol{j}$ and $\boldsymbol{E}$ described by the Hall angle $\theta_H = \arctan(\mu B)$ relative to vector of drift electric field, where μ is carriers mobility. At sufficiently high fields B, the Hall angle approaches 90°, in which case $\boldsymbol{j}$ is parallel to the semiconductor/metal interface, and the current is deflected from the metal inhomogeneities, which acts as an open circuits. Our experiments show that θ_H at $B = 8$ T is close to 60-65°, so that current routes ($\boldsymbol{j}$) are pushed out the Co particles back into graphene layer, and current routes (red lines in Figure 16c) become strongly bended and also self-crossing (due to multiplicity of Co particles). In such a case, at high B values Co particles act as an open circuits in graphene, and the current in Figure 16c flows around (skirts) them. Due to such a new system of current routes, formed by Lorentz force at high B values, their lengths strongly increase, i.e. magnetoresistance in the Co-G/SiO_2 sample grows much stronger with B as compared to the pure graphene.

Therefore, the sample Co-G/SiO_2 looks like highly inhomogeneous media (similar to metal-insulator nanocomposites [56]) with percolating character of carrier transport. We believe that this explanation allows understanding why decoration of graphene with Co particles enhances PMR effect at large magnetic fields B.

Therefore, the described crossover of the metallic particles behavior from a short circuit at low B values to an open circuit at high magnetic fields brings about a large increase in resistance, i.e. the EMR effect.

As was shown in [26-30, 54, 55], the influence of magnetic field on redistribution of current density in the graphene/metal hybrid structure is essentially a geometric interfacial phenomenon. However, contributions from intrinsic effects of the hybrid structure components should not be neglected as well. Among such intrinsic effects, which are enhanced with temperature lowering [58-60], we can note dependence of carrier mobility on magnetic field [14], formation of LSPR [14, 20, 21, 50-53], carrier mobility fluctuations [56, 57], etc. All these contributions can be associated with polycrystalline structure and/or inhomogeneous distribution of defects in twisted graphene owing to its contamination by impurities and imperfections as a result of transfer from Cu foil to SiO_2 substrate [11] and change in its electronic structure due to deposition of Co clusters, observed in our experiment.

6. Conclusions

In summary, electrochemical deposition of Co particles slightly increases the defectiveness of twisted graphene and significantly decreases surface resistivity in Co-*G*/SiO_2 samples. Observed $R_\square$ decrease evidences the formation of low-ohmic (barrier-free) electric contact between Co particles and graphene sheets. Taking into account the polycrystalline structure of *G*/SiO_2 samples, we attribute this effect to the shunting of intergrain boundaries by Co precipitates.

Modelling of experimental dependencies of surface resistance on temperature $R_\square(T)$ and magnetic field $R_\square(B)$ for *G*/SiO_2 samples and Co-*G*/SiO_2 samples proves that at the temperature range 2-20 K $R_\square(T,B)$ can be considered within the co-existence of two models: 3D Mott VRH and 2D WLQC to the Drude conductivity for weak localization conditions.

It is experimentally observed that decoration with Co particles results in negative magnetoresistance in graphene in weak magnetic fields (below 1-2 T) that originates from quantum interference effects and VRH mechanism. At the same time, the increase of positive magnetoresistance in strong magnetic fields (above 5 T) is governed with carrier transport in large-scale potential relief which possibly initiates extraordinary magnetoresistance effect in Co-*G*/SiO_2 sample. Phenomenological model is proposed which describes the different effect of Co particles onto the $R_\square(T,B)$ in twisted graphene sheets at weak and strong magnetic fields. This model basically attributes the increased contribution of PMR to the

distortion of current-conducting routes under the influence of Lorentz force due to the enhancement of LSPR in Co-*G*/SiO_2 samples.

Acknowledgements

This work was supported by the State Committee for Science and Technology of the Republic of Belarus (BRFFR project F18PLSHG-005), the State Program "Photonics, opto- and microelectronics" (project N 3.3.01) and the contract N 08626319/182161170–74 with JINR (Russian Federation). S. L. Prischepa and I.V. Komissarov acknowledge financial support of the "Improving of the Competitiveness Program" of the National Research Nuclear University MEPhI. Technical support in the preparation of the paper from bachelor A.V. Pashkevich (INP BSU) is strongly acknowledged.

References

[1] A.C. Ferrari, F. Bonaccorso, V. Fal'ko, K.S. Novoselov, S. Roche, P. Bøggild, et. al., Science and technology roadmap for graphene, related two-dimensional crystals, and hybrid systems, Nanoscale 7 (2015) 4598–4810. https://doi.org/10.1039/C4NR01600A.

[2] Y. Liu, Z. Liu, W.S. Lew, Q.J. Wang, Temperature dependence of the electrical transport properties in few-layer graphene interconnects, Nanoscale Res. Lett. 8 (2013) 335. https://doi.org/10.1186/1556-276X-8-335.

[3] A.H.C. Neto, F. Guinea, N.M.R. Peres, K.S. Novoselov, A.K. Geim, The electronic properties of graphene, Rev. Mod. Phys. 81 (2009) 109. https://doi.org/10.1103/RevModPhys.81.109.

[4] A.A. Sokolik, A.D. Zabolotskiy, Y.E. Lozovik, Many-body effects of coulomb interaction on landau levels in graphene, Phys. Rev. B 95 (2017) 125402. https://doi.org/10.1103/PhysRevB.95.125402.

[5] J. Tuček, Z. Sofer, D. Bouša, M. Pumera, K. Holá, A. Malá, K. Poláková, M. Havrdová, K. Čépe, O. Tomanec, R. Zbořil, Air-stable superparamagnetic metal nanoparticles entrapped in graphene oxide matrix, Nature Commun. 7 (2016) 12879. https://doi.org/10.1103/10.1038/ncomms12879.

[6] S. Zhidkov, N.A. Skorikov, A.V. Korolev, A.I. Kukharenko, E.Z. Kurmaev, V.E. Fedorov, S.O. Cholakh, Electronic structure and magnetic properties of graphene/Co composite, Carbon 94 (2015) 464. https://doi.org/10.1016/j.carbon.2015.04.086.

[7] Y. Khatami, H. Li, S.C. Xu, K. Banerjee, Metal-to-Multilayer-Graphene Gontact—Part I: Contact Resistance Modeling, IEEE Trans. Electron Devices 59 (2012) 2444–2452. https://doi.org/10.1109/TED.2012.2205256.

[8] J. Lenz, S. Edelstein, Magnetic sensors and their applications, IEEE Sensors Journal 6 (2006) 631–649. https://doi.org/10.1109/JSEN.2006.874493.

[9] J.M. Daughton, Y.J. Chen, GMR Materials for low field applications. IEEE Trans. Magn. 29 (1993) 2705–2710. https://doi.org/10.1109/20.280936.

[10] G. Li, V. Joshi, R.L. White, S.X. Wang, J.T. Kemp, C. Webb, R.W. Davis, S. Sun, Detection of single micron-sized magnetic bead and magnetic nanoparticles using spin valve sensors for biological applications, J. Appl. Phys. 93, (2003) 7557–7559. https://doi.org/10.1063/1.1540176.

[11] G. Ruhl, S. Wittmann, M. Koenig, D. Neumaier, The Integration of Graphene into Microelectronic Devices, Beilstein J. Nanotechnol. 8 (2017) 1056–1064. https://doi.org/10.3762/bjnano.8.107.
[12] B.L. Altshuler, A.G. Aronov, D.E. Khmelnitsky, Effects of Electron-electron collisions with small energy transfers on quantum localisation, J. Phys. C 15 (1982) 7367–7386. https://doi.org/10.1088/0022-3719/15/36/018.
[13] B.L. Altshuler, A.G. Aronov, Electron–electron interaction in disordered conductors, in Modern Problems in Condensed Matter Sciences, Elsevier 10, 1985. https://doi.org/10.1016/B978-0-444-86916-6.50007-7.
[14] B.I.Shklovskii, A.L. Efros, Electronic properties of doped semiconductors, Springer Series in Solid-State Sciences, Heidelberg, 1984, pp. https://doi.org/10.1007/978-3-662-02403-4.
[15] V.M. Pudalov, Metallic conduction, apparent metal-insulator transition and related phenomena in two-dimensional electron liquid, Societá Italiana di Fisica 157 (2004) 335–356. https://doi.org/10.3254/978-1-61499-013-0-335.
[16] R.V. Gorbachev, F.V. Tikhonenko, A.S. Mayorov, D.W. Horsell, A. Savchenko, Weak localization in bilayer graphene, Phys. Rev. Lett. 98 (2007) 176805. https://doi.org/10.1103/PhysRevLett.98.176805.
[17] K. Kechedzhi, E. Mccann, V.I. Fal'ko, H. Suzuura, T. Ando, B.L. Altshuler, Weak localization in monolayer and bilayer graphene, Eur. Phys. J. Spec. Top. 148 (2007) 39–54. https://doi.org/10.1140/epjst/e2007-00224-6.
[18] J. Jobst, D. Waldmann, I.V. Gornyi, A.D. Mirlin, H.B. Weber, Electron-electron interaction in the magnetoresistance of graphene, Phys. Rev. Lett. 108 (2012) 106601. https://doi.org/10.1103/PhysRevLett.108.106601.
[19] S.V. Morozov, K.S. Novoselov, M.I. Katsnelson, F. Schedin, D. Jiang, A.K. Geim, Strong suppression of weak localization in graphene, Phys. Rev. Lett. 97 (2006) 016801. https://doi.org/10.1103/PhysRevLett.97.016801.
[20] N.F. Mott, Conduction in non-crystalline materials, Journal of Theoretical Experimental and Applied Physics 19, (1969) 835–852. https://doi.org/10.1080/14786436908216338.
[21] N.F. Mott, E.A. Davis, Electronic processes in non-crystalline materials, second ed., University Press, Oxford, 1979. https://trove.nla.gov.au/work/9122384.
[22] B.I. Shklovskii, Hopping conductivity of semiconductors in strong magnetic fields. Semiconductors 6 (1973) 1084–1088. https://experts.umn.edu/en/publications/hopping-conduction-in-semiconductors-subjected-to-a-strong-electr.
[23] N. Mikoshiba, Weak-field magnetoresistance of hopping conduction in simple semiconductors, J. Phys. Chem. Solids 24 (1963) 341–346. https://doi.org/10.1016/0022-3697(63)90192-6.
[24] S. Pisana, P.M. Braganca, E.E. Marinero, B.A. Gurney, Graphene magnetic field sensors, IEEE Trans. Magn. 46 (2010) 1910–1913. https://doi.org/10.1109/TMAG.2010.2041048.
[25] J. Lu, H. Zhang, W. Shi, Z. Wang, Y. Zheng, T. Zhang, N. Wang, Z. Tang, P. Sheng, Graphene magnetoresistance device in van Der Pauw geometry, Nano Lett. 11 (2011) 2973–2977. https://doi.org/10.1021/nl201538m.
[26] S.A. Solin, Tineke Thio, D.R. Hines, J.J. Heremans, Enhanced Room-temperature geometric magnetoresistance in inhomogeneous narrow-gap semiconductors, Science 289 (2000) 1530–1532. https://doi.org/10.1126/science.289.5484.1530.
[27] W.R. Branford, A. Husmann, S.A. Solin, S.K. Clowes, T. Zhang, Y.V. Bugoslavsky, L.F. Cohen, Geometric manipulation of the high-field linear magnetoresistance in InSb epilayers on GaAs(001), Appl. Phys. Lett. 86, (2005) 202116. https://doi.org/10.1063/1.1923755.

[28] C. Wan, X. Zhang, X. Gao, J. Wang, X. Tan, Geometrical enhancement of low-field magnetoresistance in silicon, Nature 477 (2011) 304–307. https://doi.org/10.1038/nature10375.
[29] S.A. Solin, L.R. Ram–Mohan, Geometry-Driven Magnetoresistance, American Cancer Society, 2007. https://doi.org/10.1002/9780470022184.hmm518.
[30] D.R. Baker, J.P. Heremans, Linear geometrical magnetoresistance effect: influence of geometry and material composition, Phys. Rev. B 59 (1999) 13927–13942. https://doi.org/10.1103/PhysRevB.59.13927.
[31] I.V. Komissarov, N.G. Kovalchuk, V.A. Labunov, K.V. Girel, O.V. Korolik, M.S. Tivanov, A. Lazauskas, M. Andrulevičius, T. Tamulevičius, V. Grigaliūnas, Š. Meškinis, S. Tamulevičius, S.L. Prischepa, Nitrogen-doped twisted graphene grown on copper by atmospheric pressure CVD from a decane precursor, Beilstein J. Nanotechnol. 8 (2017) 145–158. https://doi.org/10.3762/bjnano.8.15.
[32] T.–F. Chung, Y. Xu, Y.P. Chen, Transport measurements in twisted bilayer graphene: electron-phonon coupling and landau level crossing, Phys. Rev. B 98 (2018) 035425. https://doi.org/10.1103/PhysRevB.98.035425.
[33] V.G. Bayev, J.A. Fedotova, J.V. Kasiuk, S.A. Vorobyova, A.A. Sohor, I.V. Komissarov, N.G. Kovalchuk, S.L. Prischepa, N.I. Kargin, M. Andrulevičius, J. Przewoznik, Cz. Kapusta, O.A. Ivashkevich, S.I. Tyutyunnikov, N.N. Kolobylina, P.V. Guryeva, CVD graphene sheets electrochemically decorated with "core-shell" Co/CoO nanoparticles, Appl. Surf. Sci. 440 (2018) 1252–1260. https://doi.org/10.1016/j.apsusc.2018.01.245.
[34] C.-J. Shih, A. Vijayaraghavan, R. Krishnan, R. Sharma, J.-H. Han, M.-H. Ham, Z. Jin, S. Lin, G.L.C. Paulus, N.F. Reuel, Q.H. Wang, D. Blankschtein, M.S. Strano, Bi- and trilayer graphene solutions. Nature Nanotechnol. 6 (2011) 439–445. https://doi.org/10.1038/nnano.2011.94.
[35] N.G. Kovalchuk, K.A. Nigerish, M.M. Mikhalik, N.I. Kargin, I.V. Komissarov, S.L. Prischepa, Possibility of determining the graphene doping level using Raman spectra, J Appl. Spectrosc. 84 (2018) 995–998. https://doi.org/10.1007/s10812-018-0576-x.
[36] S. Wan, H. Wan, H. Bi, J. Zhu, L. He, K. Yin, S. Su, L. Sun, A Surface transition of nanoparticle-decorated graphene films from water-adhesive to water-repellent, Nanoscale 10 (2018) 17015–17020. https://doi.org/10.1039/C8NR04831B.
[37] D.A. Mosin, N.G. Kovalchuk, A. Lazauskas, V.A. Labunov, S. Tamulevičius, S.L. Prischepa I.V. Komissarov, The Influence of Copper Solvent Type and Its Concentration on Defectiveness of Graphene Film Transferred from Catalyst on Target Substrate, Mokerov readings, Moscow, (2016) 105–110.
[38] K. Kim, S. Coh, L.Z. Tan, W. Regan, J.M. Yuk, E. Chatterjee, M. F. Crommie, Marvin L. Cohen, Steven G. Louie, and A. Zettl, Raman spectroscopy study of rotated double-layer graphene: misorientation-angle dependence of electronic structure, Phys. Rev. Lett. 108 (2012) 246103. https://doi.org/10.1103/PhysRevLett.108.246103.
[39] A.O. Sboychakov, A.L. Rakhmanov, A.V. Rozhkov, F. Nori, Electronic spectrum of twisted bilayer graphene, Phys. Rev. B 92, (2015) 075402. https://doi.org/10.1103/PhysRevB.92.075402.
[40] A.A. Lebedev, N.V. Agrinskaya, S.P. Lebedev, M.G. Mynbaeva, V.N. Petrov, A.N. Smirnov, A.M. Strel'chuk, A.N. Titkov, D.V. Shamshur, Low-Temperature transport properties of multigraphene films grown on the SiC surface by sublimation. Semiconductors 45 (2011) 623–626. https://doi.org/10.1134/S1063782611050186.
[41] A. Shaffique, M.D. Stiles, Temperature dependence of the diffusive conductivity of bilayer graphene, Phys. Rev. B 82 (2010) 075423. https://doi.org/10.1103/PhysRevB.82.075423.

[42] Z.Z. Alisultanov, R.P. Meilanov, Transport properties of epitaxial graphene formed on the surface of a superconductor, Semiconductors 48 (2014) 924–934. https://doi.org/10.1134/S1063782614070021.
[43] A.V. Butko, V.Y. Butko, Electrical transport in graphene with different interface conditions. Phys. Solid State 57 (2015) 1048–1050. https://doi.org/10.1134/S1063783415050066.
[44] E.C. Peters, Magnetotransport in Graphene: Gap-Opening and Interaction Effects, Max Planck Institute for Solid State Research, Stuttgart, 2013.
[45] R. Oppermann, M.J. Schmidt, D. Sherrington, Double criticality of the Sherrington-Kirkpatrick model at T=0, Phys. Rev. Lett. 98, (2007) 127201. https://doi.org/10.1103/PhysRevLett.98.127201.
[46] G.M. Minkov, O.E. Rut, A.V. Germanenko, A.A. Sherstobitov, V.I. Shashkin, O.I. Khrykin, V. M. Daniltsev, Quantum corrections to the conductivity in two-dimensional systems: Agreement between theory and experiment, Phys. Rev. B 64 (2001) 253327. https://doi.org/10.1103/PhysRevB.64.235327.
[47] A.V. Germanenko, G.M. Minkov, O.E. Rut, Weak localization in macroscopically inhomogeneous two-dimensional systems: a simulation approach, Phys. Rev. B 64 (2001) 165404. https://doi.org/10.1103/PhysRevB.64.165404.
[48] Y. Imry, Introduction to Mesoscopic Physics, Oxford University Press, Oxford, 1997. ISBN:978-0-19-510167-6.
[49] M. Kohler, Zur magnetischen widerstandsänderung reiner metalle, Annalen der Physik 424 (1938) 211–218. https://doi.org/10.1002/andp.19384240124.
[50] A.Y. Shik, Electronic Properties of Inhomogeneous Semiconductors, Electrocomponent Science Monographs, Amsterdam, 1995. ISSN 0275-7230.
[51] C. Herring, Effect of random inhomogeneities on electrical and galvanomagnetic measurements, J. Appl. Phys. 31 (1960) 1939. https://doi.org/10.1063/1.1735477.
[52] A.Y. Shik, Hall effect and electron mobility in inhomogeneous semiconductors, ZETP Lett. 20 (1974) 14–16. http://www.jetpletters.ac.ru/ps/1783/article_27171.pdf.
[53] A. Shik, Non-uniform two-dimensional electron gas in a magnetic field. HAIT Journal of Science and Engineering 1 (2004) 470. https://pdfs.semanticscholar.org/ae23/9aa1043b658db39032cafe68bb6082169212.pdf.
[54] A.C.H. Rowe, S.A. Solin, Importance of interface sampling for extraordinary resistance effects in metal semiconductor hybrids, Phys. Rev. B 71 (2005) 235323. https://doi.org/10.1103/PhysRevB.71.235323.
[55] Jian Sun and Jürgen Kosel, Extraordinary Magnetoresistance in Semiconductor/Metal Hybrids: A Review, Materials, 6, (2013) 500. https://doi.org/10.3390/ma6020500
[56] A.M. Saad, A.K. Fedotov, J.A. Fedotova, I.A. Svito, B.V. Andrievsky, Yu.E. Kalinin, et al, Characterization of $(Co_{0.45}Fe_{0.45}Zr_{0.10})_x(Al_2O_3)_{1-x}$ nanocomposite films applicable as spintronic materials, Phys. Stat. Solidi (c) 3, (2006) 1283. https://doi.org/10.1002/pssc.200563111.
[57] A.A. Abrikosov, Quantum magnetoresistance, Phys. Rev. B 58 (1998) 2788–2794. https://doi.org/10.1103/PhysRevB.58.2788.
[58] Y.-B. Zhou, B.-H. Han, Z.-M. Liao, H.-C. Wu, D.-P. Yu, From positive to negative magnetoresistance in graphene with increasing disorder, Appl. Phys. Lett. 98 (2011) 222502. https://doi.org/10.1063/1.3595681.
[59] J.S. Hu, T.F. Rosenbaum, Classical and quantum routes to linear magnetoresistance. Nature Mater. 7 (2008) 697–700. https://doi.org/10.1038/nmat2259.
[60] M.M. Parish, P.B. Littlewood, Non-saturating magnetoresistance in heavily disordered semiconductors. Nature 426 (2003) 162. https://doi.org/10.1038/nature02073.

Conflict of interests

We have no conflict of interests

Dear A Somasundaram
I repeat my correspondence with you and your colleague Gopal. I have answered on all your questions (see, letters below).
1) Article reference number: PHYSE 113790
2) Highlights

- Distributed shunts and high-quality low-ohmic Co electrodes are formed on twisted CVD graphene (G) sheets by decoration with Co particles for application in magnetic sensing devices.
- The crossover from negative to positive magnetoresistance in Co-G/SiO2 samples at weak and strong magnetic fields, correspondingly, are considered within the phenomenological model assuming the additional distortion of current-conducting routes under the influence of Lorentz force due to the enhancement by Co particles of large-scale potential relief.

Best regards,
A. Fedotov